http://dx.doi.org/10.11142/jicems.2013.2.1.1
Journal of International Conference on Electrical Machines and Systems Vol. 2, No. 1, pp. 1 ~8 , 2013

Comparison of Three Magnet Array-type Rotors in Surface Permanent Magnet-type Vernier Motor

Yasuhiro Kataoka *, Masakazu Takayama *, Yoshitarou Matsushima ** and Yoshihisa Anazawa *

Abstract – **Surface permanent magnet-type vernier motors with three magnet array-type rotors (parallel magnetized type, repulsion type, and Halbach type) are compared based on the pull-out torque. It was clarified that increasing the rotor radius increases the pull-out torque at a fixed three-phase alternating voltage. The mechanism for the pull-out torque increase on each magnet array type was different, when the effects of the increase were analyzed based on an induced electromotive force and a synchronous reactance. As a result, the design of the Halbach-type rotor was found to be especially effective for achieving high pull-out torque, because this array type achieves a large induced electromotive force E_0 and a small synchronous reactance x_s.**

Keywords: **Halbach array, Repulsion array, Pull-out torque, Vernier motor**

1. Introduction

A surface permanent magnet (SPM)-type vernier motor is a synchronous motor that runs at a slow speed and generates a high torque without a reduction gear. Therefore, a direct-drive system operated with this motor has advantages such as high-resolution positioning (non-backlash), low friction loss and no maintenance. Moreover, the vernier motor theoretically can have a non-cogging torque. So, this motor is suitable for direct-drive systems, and has been developed to increase the output torque [1].

In the SPM-type vernier motor, a small displacement of the rotor produces a large displacement of the magnetic field [2]; therefore, a large induced electromotive force is obtained at a slow speed and a high torque can be generated. To increase the induced electromotive force, the magnetic flux that is interlinked to the armature windings should be increased. Generally, a repulsion-type and a Halbach-type magnet array are used to increase the magnetic flux generating at the surface of magnet [3], [4].

In the SPM-type vernier motor, the magnetic flux, produced by the field magnets of the rotor, is modulated by a magnetic gap permeance wave, and the modulated magnetic flux is interlinked to the armature windings. The effect of this magnetic modulation depends on the magnetic structure around the gap [5]. In this paper, the following three magnet array-type rotors are compared according to the pull-out torque:

1) Parallel magnetized array type (standard type)
2) Repulsion array type
3) Halbach array type

The pull-out torques on each array type are calculated by the γ-δ axis torque equation, which includes the induced electromotive force and the synchronous reactance. Additionally, these two elements are calculated using a 2 dimensional finite element analysis (2D FEA). It is found that when the rotor radius of these three magnet array types is increased 1.5-fold, the pull-out torque is increased 1.5-fold at a fixed alternating voltage of 125 V. However, the mechanism for the pull-out torque increase on each magnet array type is different. The results indicate that the design of the Halbach array type is especially effective for achieving high pull-out torque.

2. Structure and Operational Principle

The effects of the rotor radius are investigated using an inner-rotor type vernier motor. The vernier structure, the three magnet array-type rotors, the specifications, and the operational principle of the SPM-type vernier motor are described in this section.

* Dept. of Electronics and Information Systems, Akita Prefectural University, Japan. (yasuhiro_kataoka@akita-pu.ac.jp, masat@akita-pu.ac.jp, anazawa@akita-pu.ac.jp)
** Dept. of Electrical and Electronic Engineering, Shizuoka University, Japan. (teymats@ipc.shizuoka.ac.jp)
Received12 November 2012 ; Accepted 15 January 2013

2.1 Structure of the SPM-type Vernier Motor

A 2-pole section of the SPM-type vernier motor is shown in Fig. 1. The stator has 36 slots and ordinary three-phase armature windings, and generates 12 magnetic poles. The number of slots per pole per phase is 1. The rotor with the field magnets has 60 magnetic poles. In the SPM-type vernier motor, the number of slots S, poles P on the primary side, and field poles R on the secondary side are constructed based on the principle of the vernier, and the relationship between these parameters is shown in equation (1).

$$S = \frac{R}{2} \pm \frac{P}{2} \tag{1}$$

The rotor radius r_o is increased from 89.7 to 134.7 mm (a 1.5-fold increase), where the gap length of 0.3 mm and the stator thickness of 65 mm are not changed. The tooth width and the open slot width are set to be equal at the gap side.

The three magnet array-type rotors are shown in Fig. 2. In the parallel magnetized array type (Fig. 2-a), 60 pieces of magnets, which are magnetized parallel in the direction of the rotor radius axis, are arranged on the surface of the rotor. Additionally, the demagnetization area is set at a width of $\tau_p/4$ on both sides of a magnet piece (τ_p is the pole pitch of the field magnets), and the rotor core is made of electrical steel sheet (50A290). In the repulsion array type (Fig. 2-b), 60 pieces of magnets, which are magnetized in the direction of the circumferential axis, are arranged. A demagnetization area is not set, and the rotor core is made of a non-magnetic material. In the Halbach array type (Fig. 2-c), 120 pieces of magnets, which are magnetized in the Halbach pattern [3], are arranged. The width of the magnet pieces is $\tau_p/2$. A demagnetization area is not set, and the rotor core is made of a non-magnetic material.

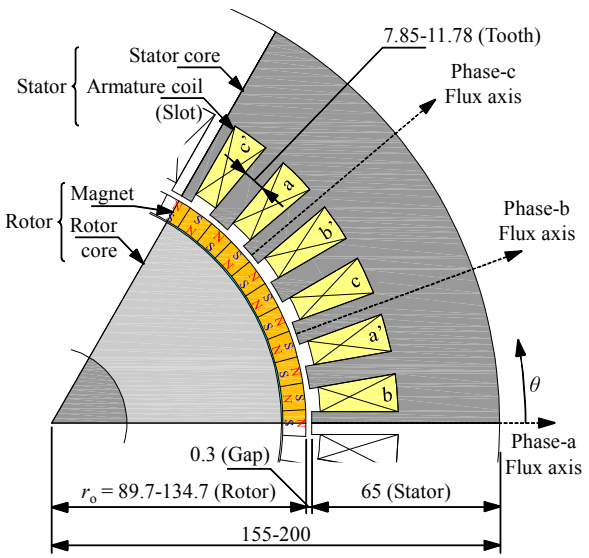

Fig. 1. 2-pole section of SPM-type vernier motor. (Units: mm)

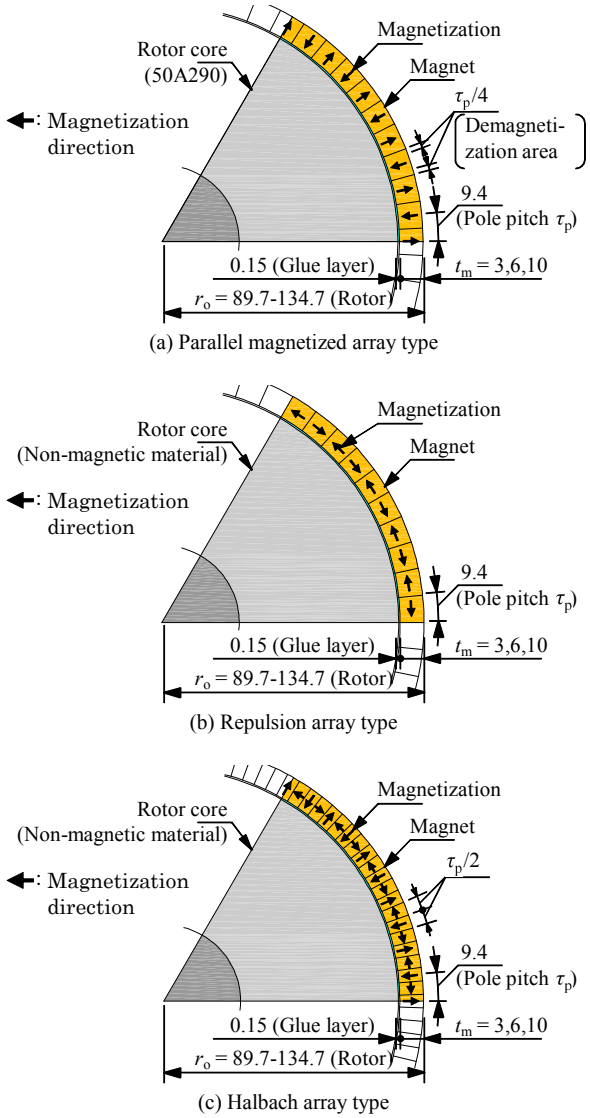

Fig. 2. Three magnet array-type rotors. (Units: mm)

The specifications are shown in Table 1. The magnets in these array-type rotors are Nd-Fe-B rare earth magnets. The thickness of the magnets is 3 mm, 6 mm, and 10 mm, and the effects of the rotor radius are calculated for each magnet thickness. The core length is 60 mm.

2.2 Operational Principle

The operational principle of the SPM-type vernier motor

is shown in Fig. 3. This motor is driven by a three-phase alternating voltage, and a rotating magnet field is generated in the gap of the motor. In this structure, the 5th harmonic wave of the rotating magnetic field is produced by the magneticmotive force of the three-phase armature windings and the magnetic gap permeance wave. The rotor rotates slowly while synchronizing the 5th harmonic wave of the rotating magnetic field, because the rotor has 60 magnetic poles. Therefore, the rotor speed is stepped down to 1/5 of the speed of the rotating magnetic field, and the torque is stepped up. Thus this motor works as a motor with magnetic gearing. The rotor speed is shown in equation (2):

$$N = \frac{120f}{P} \cdot \frac{P}{R} = \frac{120f}{R} \tag{2}$$

where N is the synchronous speed (min^{-1}), and f is the power supply frequency (Hz).

Table 1. Specifications of SPM-type vernier motor

Items		Value	
Magnet	Residual induction	1.45	T
	Coercive force	1074	kA/m
Core	Length	60	mm
	Material (Primary side)	50A290	–
Armature coil	Turns	336	Turn
	Winding	Full pitch	–
Power supply	Line voltage	125	V
	Frequency	50	Hz

3. Calculation Method of the Torque

The pull-out torque is calculated by a torque equation on the γ-δ axis. This torque equation includes elements of the induced electromotive force and the synchronous reactance. Therefore, the effects of a pull-out torque increase can be analyzed easily.

3.1 γ-δ Axis Torque Equation

The torque equation is given in equation (3), when a field magnet is treated as an equivalent coil [6]:

$$T = -\left(\frac{R}{2}\right) M_{\mathrm{F}} I_{\mathrm{F}} I_{\delta} \tag{3}$$

where T is the torque (N-m), $M_{\mathrm{F}}I_{\mathrm{F}}$ is the interlinkage magnetic flux (Wb), and I_{δ} is the current on the δ axis (A).

When balanced steady-state operation is considered, the voltage equations on the γ-δ axis and the induced electromotive force equation are given in equations (4), (5) and (6) [6]:

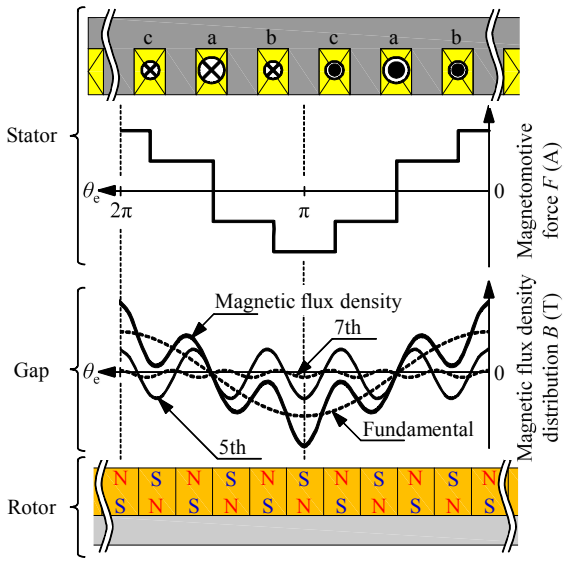

Fig. 3. Operational principle of SPM-type vernier motor. (Units: mm)

$$V\sin\left(\frac{R\delta_{\mathrm{L}}}{2}\right) = -r_{\mathrm{a}} I \sin\left(\varphi - \frac{R\delta_{\mathrm{L}}}{2}\right) + x_{\mathrm{s}} \cos\left(\varphi - \frac{R\delta_{\mathrm{L}}}{2}\right) \tag{4}$$

$$V\cos\left(\frac{R\delta_{\mathrm{L}}}{2}\right) = x_{\mathrm{s}} \sin\left(\varphi - \frac{R\delta_{\mathrm{L}}}{2}\right) + r_{\mathrm{a}} I \cos\left(\varphi - \frac{R\delta_{\mathrm{L}}}{2}\right) + E_0 \tag{5}$$

$$E_0 = \frac{\omega}{\sqrt{3}} M_{\mathrm{F}} I_{\mathrm{F}} \tag{6}$$

where V is the power supply voltage (V), r_{a} is the resistance of the armature winding coil (Ω), x_{s} is the synchronous reactance (Ω), φ is the power factor angle (rad), $R\delta_{\mathrm{L}}/2$ is the load angle (rad), I is the current (A), E_0 is the induced electromotive force (V), and ω is the power supply angular frequency (rad/s).

The currents on the γ and δ axis, given in equations (7) and (8), are obtained by transforming equations (4) and (5), respectively. The γ-δ axis torque equation is given in equation (9):

$$I\sin\left(\varphi - \frac{R\delta_{\mathrm{L}}}{2}\right) = \frac{V}{Z}\sin\left(\varphi_{\mathrm{s}} - \frac{R\delta_{\mathrm{L}}}{2}\right) - \frac{E_0}{Z}\sin\varphi_{\mathrm{s}} = -\frac{I_{\gamma}}{\sqrt{3}} \tag{7}$$

$$I\cos\left(\varphi - \frac{R\delta_{\mathrm{L}}}{2}\right) = \frac{V}{Z}\cos\left(\varphi_{\mathrm{s}} - \frac{R\delta_{\mathrm{L}}}{2}\right) - \frac{E_0}{Z}\cos\varphi_{\mathrm{s}} = -\frac{I_{\delta}}{\sqrt{3}} \tag{8}$$

$$T = \frac{3}{\omega}\frac{R}{2}\left\{\frac{VE_0}{Z}\cos\left(\varphi_{\mathrm{s}} - \frac{R\delta_{\mathrm{L}}}{2}\right) - \frac{E_0^2}{Z}\cos\varphi_{\mathrm{s}}\right\} \tag{9}$$

where $Z = \sqrt{r_a^2 + x_s^2}$, $\varphi_s = \tan^{-1}(x_s / r_a)$, and I_γ is the current on the γ axis (A).

The torque of the SPM-type vernier motor can be calculated by equation (9), after the induced electromotive force E_0 and the synchronous reactance x_s are calculated. It is found that the pull-out torque is proportional to E_0 and inversely proportional to x_s.

3.2 Calculation of the Pull-out Torque

The procedure of the pull-out torque calculation is shown in Fig. 4.

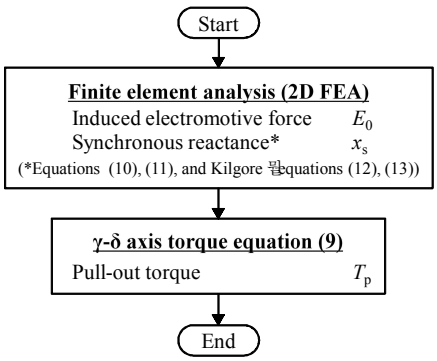

Fig. 4. Procedure of pull-out torque calculation.

In the first step, the induced electromotive force E_0 and the synchronous reactance x_s are calculated by finite element analysis (FEA, JMAG-studio Ver. 10.0). The induced electromotive force E_0 is the fundamental wave root-mean-square (RMS) value of the harmonic analysis for the phase-a voltage waveform. The synchronous reactance x_s is calculated by equations (10) - (13):

$$x_s = x_a + x_l \tag{10}$$

$$x_a = \omega L = \omega \frac{\psi}{i} \tag{11}$$

$$x_l = X\lambda_e = X\frac{4}{l}(2l_{e2} + l_{e1}) \tag{12}$$

$$X = 40flm(2p)\left(q\frac{n_s}{c}k_p k_d\right)^2 \times 10^{-8} \tag{13}$$

where x_a is the reactance of the armature reaction (Ω), x_l is the leakage reactance (Ω), L is the inductance (H), ψ is the interlinked magnetic flux (Wb), i is the line current (A), X is the leakage coefficient, λ_e is the coil-end length (m), l is the core length (m), m is the number of phases, p is the number of pole pairs, q is the number of slots per pole per phase, n_s is the number of coil sides in a slot, c is the number of parallel circuits per phase (=1), k_p is the short-pitch factor (=1), and k_d is the distribution factor (=1).

The interlinked magnetic flux ψ for the armature windings of phase-a is calculated by 2D FEA, when the line current i for the phase-a is 10 A ($i_a = -2i_b = -2i_c$), and the reactance of the armature reaction x_a is calculated by equation (11). Additionally, the armature reaction x_a is corrected by the leakage reactance x_l, which is the reactance by the coil-end leakage flux and is calculated by Kilgore's equations (12), (13) [7], because the leakage reactance x_l cannot considered in the 2D FEA. The calculation results of the coil specifications are shown in Table 2.

Table 2. Calculation results of coil specifications

Rotor inside radius r_o (mm)		89.7	104.7	119.7	134.7
Size of coil end	l_{e1} (mm)	55.8	63.6	71.5	79.3
	l_{e2} (mm)	18.7	18.7	18.7	18.7
Coil-end leakage reactance x_l (Ω)		0.84	0.91	0.98	1.1
Resistance of coil* r_a (Ω)		0.85	0.77	0.73	0.69

* Packing factor in the slot is 50.7 %.

In the next step, the torque is calculated by equation (9), and the pull-out torque is the maximum torque, which is calculated depending on the load angle.

4. Effects of the Magnet Array Type

The pull-out torques for the three magnet array-type rotors are calculated and analyzed by using the induced electromotive force E_0 and the synchronous reactance x_s. The effects of the rotor radius increase are also investigated.

4.1 Characteristics of the Induced Electromotive Force

The characteristics of the induced electromotive force E_0 versus the rotor radius are shown in Fig. 5. For the parallel magnetized array type (Fig. 5-a), the induced electromotive force E_0 of magnet thickness 3 mm increases from 45.2 to 77.9 V (a 1.7-fold increase), when the rotor radius is increased from 89.7 to 134.7 mm (a 1.5-fold increase). The magnetic flux line of the parallel magnetized array type in the analysis of the induced electromotive force is shown in Fig. 6. A cross-sectional area of teeth, which face the gap, is proportional to the rotor radius; therefore, the gap permeance increases 1.5-fold. However, the permeance for the zigzag leakage flux is inversely proportional to the rotor radius [8]. Therefore, a 1.7-fold increase is obtained for the magnet thicknesses 3, 6, and 10 mm.

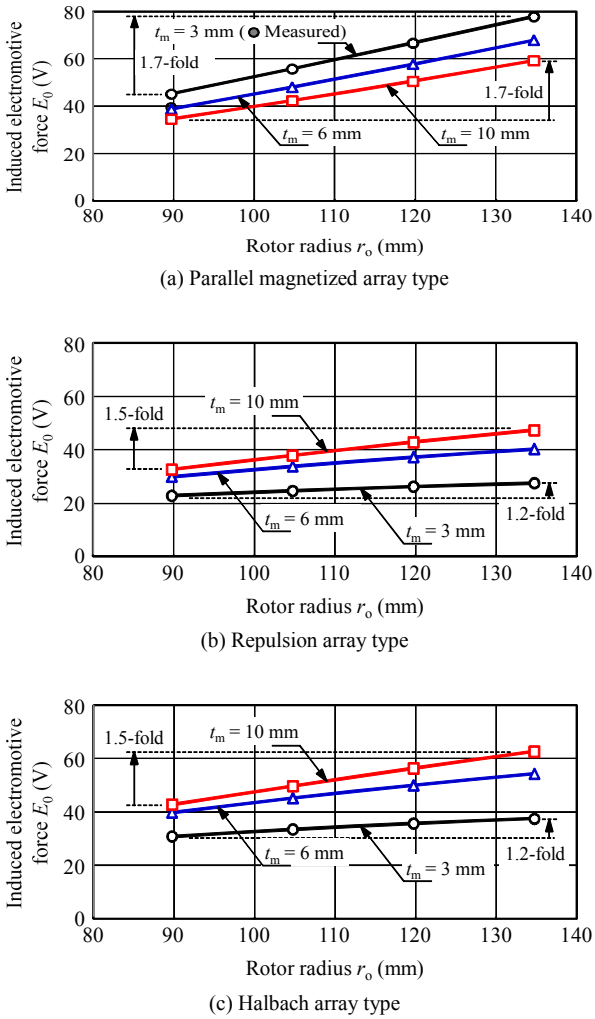

Fig. 5. Induced electromotive force versus rotor radius.

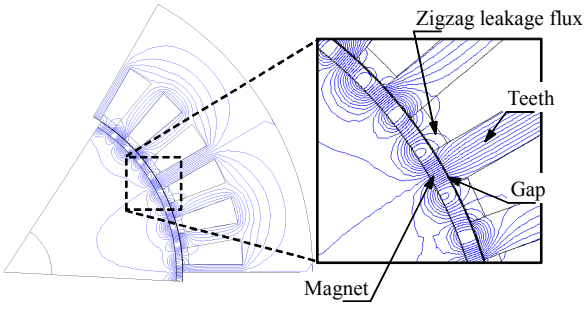

Fig. 6. Magnetic flux line of parallel magnetized array type in analysis of induced electromotive force. (r_o = 89.7 mm, t_m = 3 mm, 0.5 mWb/line)

In contrast, the induced electromotive force E_0 decreases when the magnet thickness is increased from 3 to 10 mm. The harmonics of the gap magnetic flux density distribution in the analysis of the induced electromotive force are shown in Fig. 7. The fundamental wave for the gap magnetic flux density distribution is decreased when the magnet thickness is increased from 3 to 10 mm, because the effect of magnetic modulation depending on the magnetic gap permeance wave is decreased by increasing the equivalent gap length (gap + magnet thickness). When the magnet thickness 3 mm is considered, a large induced electromotive force E_0 is obtained compared with the other array types.

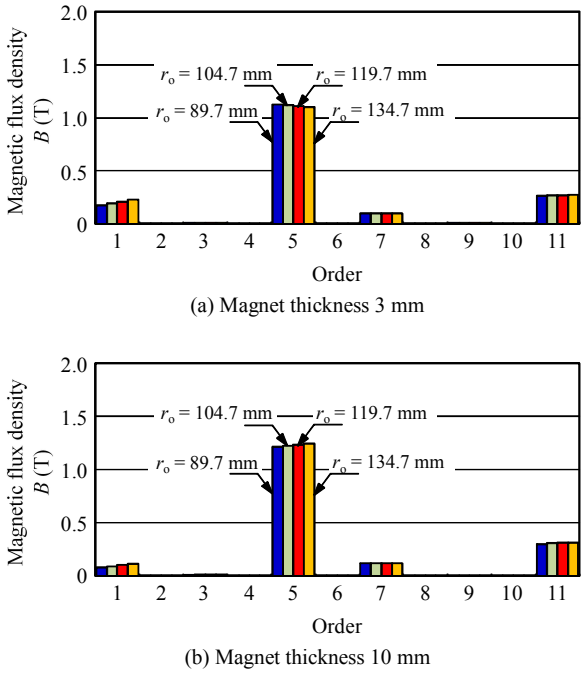

Fig. 7. Harmonics of gap magnetic flux density distribution for parallel magnetized array type in analysis of induced electromotive force.

For the repulsion array type (Fig. 5-b) and the Halbach array type (Fig. 5-c), the induced electromotive force E_0 of the magnet thickness 10 mm increases 1.5-fold when the rotor radius is increased 1.5-fold, because the gap permeance increases 1.5-fold. For the Halbach array type, when the magnet thickness 10 mm is considered, a large induced electromotive force E_0 is obtained compared with the other array types. However, the induced electromotive force E_0 of magnet thickness 3 mm increases 1.2-fold, because the cross-sectional area for the magnetic path in the magnet, which is magnetized in the circumferential direction, is narrow depending on the magnet thickness, as shown in Fig. 8. The harmonics of the gap magnetic flux density distribution are shown in Fig. 9 and Fig. 10. When the magnet thickness is increased, the 5th wave increases. However, the fundamental wave is small compared with the parallel magnetized array type. The effect of magnetic

modulation depending on the magnetic gap permeance wave is decreased because the rotor core are made of non-magnetic material.

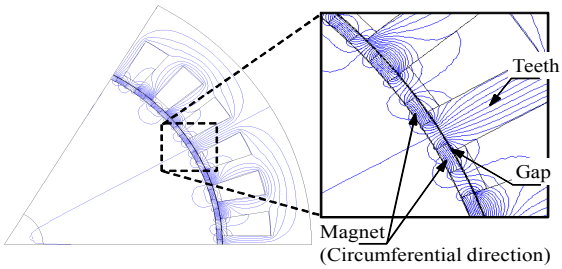

Fig. 8. Magnetic flux line of Halbach array type in analysis of induced electromotive force. (r_o = 134.7 mm, t_m = 3 mm, 0.5 mWb/line)

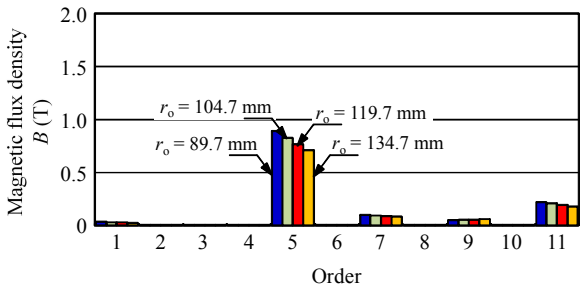

(a) Magnet thickness 3 mm

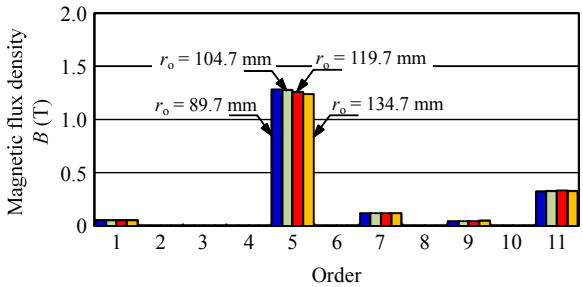

(b) Magnet thickness 10 mm

Fig. 9. Harmonics of gap magnetic flux density distribution at repulsion array type in analysis of induced electromotive force.

4.2 Characteristics of the Synchronous Reactance

The characteristics of the synchronous reactance x_s versus the rotor radius are shown in Fig. 11. For the parallel magnetized array type, the synchronous reactance x_s of magnet thickness 3 mm increases from 5.3 to 6.5 Ω (a 1.2-fold increase), when the rotor radius is increased 1.5-fold. Though the permeance in the gap increases, the permeance in the slot decreases depending on the rotor radius increase, because the slot width is increased [8].

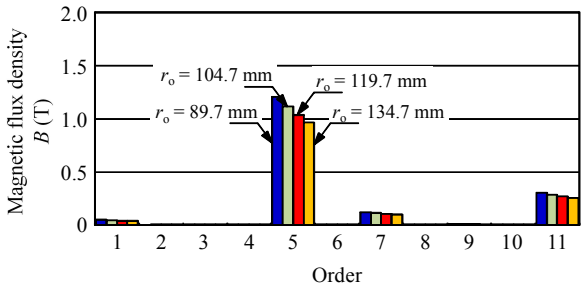

(a) Magnet thickness 3 mm

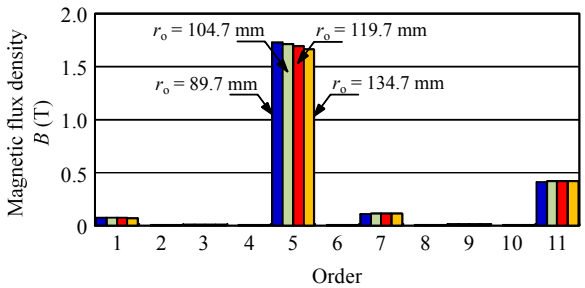

(b) Magnet thickness 10 mm

Fig. 10. Harmonics of gap magnetic flux density distribution of Halbach array type in analysis of induced electromotive force.

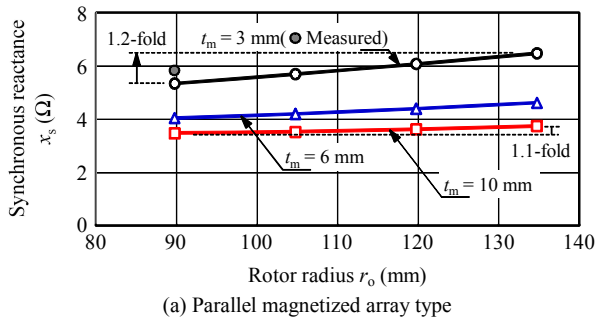

(a) Parallel magnetized array type

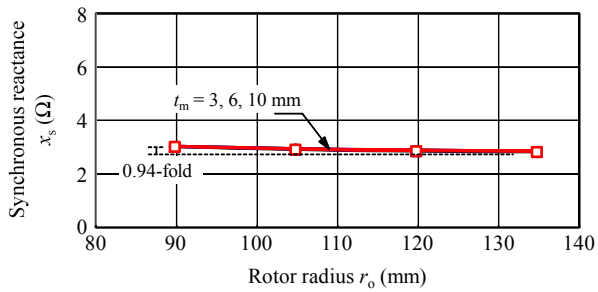

(b) Repulsion array type, Halbach array type

Fig. 11. Synchronous reactance versus rotor radius.

For the repulsion array type and the Halbach array type, the synchronous reactance x_s is 3.0 Ω at the rotor radius of 89.7 mm and decreases to 2.8 Ω, when the rotor radius is

increased to 134.7 mm, because the open slot width is increased. The synchronous reactance x_s of these array types is small compared with that of the parallel magnetized array type, because the rotor core are made of non-magnetic material.

4.3 Characteristics of the Pull-out Torque

The characteristics of the pull-out torque versus the rotor radius are shown in Fig. 12. In all array types, when the magnet thickness is 10 mm, a high pull-out torque is obtained.

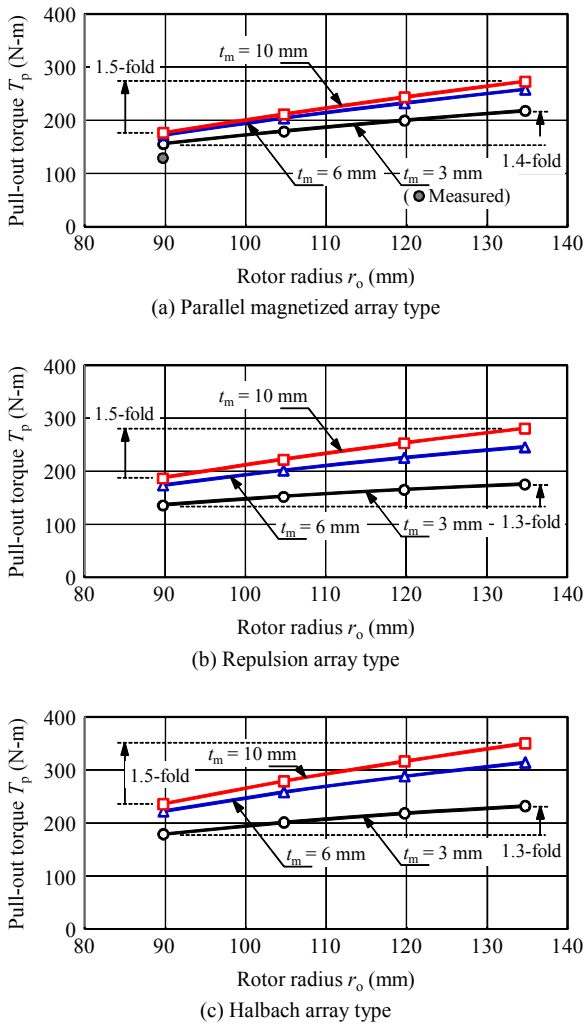

Fig. 12. Pull-out torque versus rotor radius.

When the rotor radius increases from 89.7 to 134.7 mm (a 1.5-fold increase), the pull-out torque of the magnet thickness 10 mm increases from 177 to 274 N-m (a 1.5-fold increase) for the parallel magnetized array type (Fig. 12-a). This increase is obtained by a 1.7-fold increase of the induced electromotive force E_0 and a 1.1-fold small increase of the synchronous reactance x_s. The pull-out torque of the magnet thickness 3 mm increases from 156 to 218 N-m (a 1.4-fold increase). In the parallel magnetized array type, the induced electromotive force E_0 and the synchronous reactance x_s increase when the rotor radius increases.

For the repulsion array type (Fig. 12-b), the pull-out torque of magnet thickness 10 mm increases from 188 to 282 N-m (a 1.5-fold increase), when the rotor radius is increased from 89.7 to 134.7 mm (a 1.5-fold increase). The pull-out torque increase is obtained by a 1.5-fold increase of the induced electromotive force E_0 and a 0.94-fold decrease of the synchronous reactance x_s. The pull-out torque of magnet thickness 3 mm increases from 137 to 176 N-m (a 1.3-fold increase).

For the Halbach array type (Fig. 12-c), the pull-out torque of the magnet thickness 10 mm increases from 236 to 350 N-m (a 1.5-fold increase), when the rotor radius is increased from 89.7 to 134.7 mm (a 1.5-fold increase). The pull-out torque increase is obtained by a 1.5-fold large increase of the induced electromotive force E_0 and a 0.94-fold decrease of the synchronous reactance x_s. The pull-out torque of magnet thickness 3 mm increases from 179 to 232 N-m (a 1.3-fold increase).

In the repulsion array type and the Halbach array type, the synchronous reactance x_s is decreased and the induced electromotive force E_0 is increased in contrast, when the rotor radius increases.

5. Conclusion

In this paper, three magnet array type for the SPM-type vernier motor were compared according to the pull-out torque. As a result, high torque was obtained for the Halbach array type, and its design was found to be especially effective for achieving high pull-out torque.

When the rotor radius was increased from 89.7 to 134.7 mm (a 1.5-fold increase) at the magnet thickness 10 mm, the pull-out torque increased from 177 to 274 N-m (a 1.5-fold increase) in the parallel magnetized array type. This increase was obtained by a large 1.7-fold increase of the induced electromotive force E_0 and a small 1.1-fold increase of the synchronous reactance x_s.

In the repulsion array type, the pull-out torque increased from 188 to 282 N-m (a 1.5-fold increase), when the rotor radius was increased at the magnet thickness 10 mm. In the Halbach array type, the pull-out torque increased from 236 to 350 N-m (a 1.5-fold increase). In the repulsion array type

and the Halbach array type, the reduction of the synchronous reactance x_s was influenced. Additionally, the large induced electromotive force E_0 was also obtained in the Halbach array type.

In the future, author will consider an optimal design of Halbach array-type rotor.

References

[1] A. Toba et al. : "Design and Experimental Evaluation of 5kW-Surface Permanent Magnet Vernier Machines," T.IEE Japan, Vol. 122-D, No. 2, pp. 162-168 (2002-2) (in Japanese).
[2] C. H. Lee: "Vernier Motor and Its Design," IEEE Winter General Meeting, pp. 343-349, June (1963).
[3] K. Halbach: "Design of Permanent Multipole Magnets with Oriented Rare Earth Cobalt Material," Nucl. Instrum. Methods, Vol. 169, pp. 1-10 (1980).
[4] J. C. Mallinson: "One-sided Fluxes -- A Magnetic Curiosity?", IEEE Trans. Magn., Vol. MAG-9, pp. 678-682 (1973).
[5] Y. Kataoka et al. : "Effects of Array Magnet on Pull-out Torque in Surface Permanent Magnet Type Vernier Motor," The Papers of the Technical Meeting on Rotating Machinery, IEE Japan, RM-11-98 (2011-10) (in Japanese).
[6] H. Suda et al. : "A Study of Analysis and Characteristic of Surface Permanent Magnet Vernier Motor," The Papers of the Technical Meeting on Rotating Machinery, IEE Japan, RM-07-33 (2007-5) (in Japanese).
[7] IEE Japan, "Design of electric machine," 2nd edition, pp. 331-333 (1982) (in Japanese).
[8] S. Takita et al. : "Design of High Torque Surface Permanent Magnet Type Vernier Motor," The Papers of the Technical Meeting on Rotating Machinery, IEE Japan, RM-11-97 (2011-10) (in Japanese).

Yasuhiro Kataoka received Dr. Eng. degree from Shinshu University, Nagano, Japan, in 2003. He joined Tamagawa seiki Co. Ltd. from 2003 to 2010. Since 2010, he has been an Assistant Professor at the Akita Prefectural University. His research interests include analysis and design of electric machines.

Masakazu Takayama received Dr. Eng. degree from Tohoku University in 1991. Since 2000, he has been an Associate Professor at Akita Prefectural University. His research interests are applications of electromagnetic engineering.

Yoshitarou Matsushima received B.S degree in electrical engineering from Muroran Institude of Technology in 1975 and M.E degree from Hokkaido University in 1977. He is now an associate professor at Shizuoka University. His research interests are analysis and design of electric machines.

Yoshihisa Anazawa received Dr. Eng. degree from Hokkaido University in 1987. He became a lecturer in 1980, an Associate Professor in 1989 at the Akita University. Since 1999, he has been a Professor in Akita Prefectural University. His research interests include analysis and design of electric machines.